The micro Fourier Transform Interferometer (μFTIR) - A New Field Spectrometer for Acquisition of infrared Data of Natural Surfaces

Simon J. Hook and Anne B. Kahle

Jet Propulsion Laboratory

California Institute of Technology

Pasadena, CA 911 09

Abstract

A lightweight, rugged, high-spectral-resolution interferometer has been built by Designs and Prototypes based on a set of specifications provided by the Jet Propulsion Laboratory and Dr. J. W. Salisbury (Johns Hopkins University). The instrument, the micro Fourier Transform Interferometer (μFTIR), permits the acquisition of infrared spectra of natural surfaces. Such data can be used to validate low and high spectral resolution data acquired remotely from aircraft and spacecraft in the 3-5 μm and 8-14 μm atmospheric windows. The instrument has a spectral resolution of ~6 wavenumbers, weighs 16 kg including batteries and computer, and can be operated easily by two people in the field. Laboratory analysis indicates the instrument is spectrally calibrated to better than 1 wavenumber and the radiometric accuracy is < 0.5K if the radiances from the blackbodies used for calibration bracket the radiance from the sample. Several examples of field spectra are provided for a variety of rock types, minerals and vegetation.

1. introduction

Numerous studies have successfully demonstrated the use of spaceborne remotely sensed thermal

infrared radiance data in a wide variety of disciplines such as ecology, geology and hydrology. Some of these studies have utilized data from the Advanced Very High Resolution Radiometer (AVHRR) and Along Track Scanning Radiometer (ATSR). Both of these instruments have two channels in the thermal infrared. Data from airborne radiometers with many channels in the thermal infrared have also been available for several years, e.g. the Thermal Infrared Multispectral Scanner (TIMS) and the Moderate Resolution imaging Spectrometer (MODIS) airborne simulator (MAS). However, these aircraft data are only available for a limited number of sites with a modest range of cover types, primarily due to acquisition costs and limited access. In the near future, data with similar spectral and coarser spatial resolutions as the TIMS and MAS will be available globally from two imaging instruments: MODIS and the Advanced Spaceborne Thermal Emission and Reflectance Radiometer (ASTER) on board the Earth Observing System AM Platform to be launched in 1998. In order to validate fully the results from the analysis of data acquired by these instruments it will be necessary to measure the radiance from the surface at even higher spectral resolutions with field instruments. Field measurements avoid disturbance of the natural setting which occurs when samples are transported to the laboratory. The continued need for *in situ* validation has led to the development of a few portable spectrometers.

One early instrument, developed at the Jet Propulsion Laboratory, was the Portable Field Emission Spectrometer (PFES). This instrument operated between 5 and 14.5 μm, had a spectral resolution of ~2% of the wavelength, weighed 30 kg and required a two-or three-person team for field operation (Hoover and Kahle, 1987). Recently, a replacement to that instrument has been developed by Designs and Prototypes (Tulloch, 1994) based on a set of specifications provided by

the Jet l'repulsion Laboratory and Dr. J. W. Salisbury (Salisbury, 1990; Korb et al., *submitted*). The new instrument termed the micro Fourier Transform 1 nterferometer (p FTIR) operates between 2 and 14 µm, has a spectral resolution of 6 wave numbers (wn), weighs 16 kg and ideally requires two people for field operation, although it is possible for an individual to operate the instrument.

A prototype version of the instrument was delivered to the Jet Pi opulsion Laboratory in April, 1992 and has been periodically modified based on the results of field tests. The instrument is now considered operational. The p FTIR hardware and its operation are described below together with an evaluation of the cliometric and spectral calibration of the instrument. Example spectra for a variety of surface materials are also presented. Note that although the instrument operates in both the 3-5 pm and 7-14 µm regions, this study only evaluates data from the 7-14 pm region where the majority of instruments, both airborne and spaceborne, currently have several channels or will have in the near future.

11. instrument Description

The µFTIR consists of two main components: a tripod- mounted optical head and a system unit set in a aluminium briefcase. (Figure 1). The optical head weighs 4.1 kg, and includes the interferometer, detector/dewar assembly and the optics for measuring and observing the surface. The interferometer consists of a refractively scanned cavity driven by a mass-balanced torque motor. The refractively scanned crystals of the interferometer are made of Potassium Chloride (KC]) and sealed under nitrogen pressure. There are two inter-changeable detector/dewar

assemblies, an Indium Antimonide (InSb) assembly for the 2-5 μm region and Mercury Cadmium Telluride (I IgCdTe) assembly fort the 5 to14 μm region. Both detectors are liquid-nitrogen cooled. The HgCdTe detector is doped in order to increase its sensitivity at longer wavelengths. The viewing optics are made from Zinc Selenide and the detector lens focal length is 2.5 cm. The image of the surface may be alternately projected onto the detector or onto an aiming eyepiece. The optical head is tripod-mounted; if the entrance aperture is 1 m above the surface the imaged area should be 7.6 cm in diameter, however, Korb et al. *submitted* found the infrared imaged area to be about twice as large as the 7.6 cm in diameter specified by the manufacturer. The temperature of the optical head is maintained by a theme-electric cooler. The set point for the thermoelectric cooler is 250 C; however, the equilibrium point will be slightly higher or lower depending on the ambient temperature. Data acquired by the instrument are radiometrically calibrated with the aid of a small temperature controlled blackbody which mounts on the front of the fore-optics. Calibration requires measurement of the blackbody at a minimum of two temperatures in order to determine the gain and offset. Spectral calibration is achieved using a diode laser.

The system unit, excluding the laptop computer, weights 6.4 kg and contains three main boards: a scan-servo and housekeeping board, an analogue-to-digital board and a digital signal-processor board. The interferogram is converted to a spectrum in the system unit and send out to the laptop computer via an expansion bus. There are several temperature sensors in the optical head for monitoring purposes. The output from these sensors are displayed on I. Cl] panels mounted on the system unit. The system unit is also used to set the temperature of the blackbody. The system is

connected by three cables: the battery-to-sy stem unit cable, the system unit to optical head cable and the system unit to blackbody cable (Figure 1). The entire system (excluding the laptop computer) is powered by a single re-chargeable 12 V Gel Cell that weighs 2.5 kg. The laptop computer is powered by re-chargeable Nickel Cadmium batteries and weighs 3.2 kg.

Designs and Prototypes includes a MS-DOS software package for the acquisition and analysis of the data. The software allows a set of measurements to be reduced to emissivity in near real-time.

111. Field operation

The optical head is maintained at a steady temperature by a thermo-electric cooler. The thermo-electric cooler can be powered from a vehicle's cigarette lighter en route to a drop-off point before hiking to a test site. If the optical head is not cooled until arriving at the test site it is necessary to run the thermo-electric cooler for approximately 30 minutes to stabilize the temperature of the optical head. If the optical head is not allowed to stabilize there can be a significant difference in the temperature of the head between the time the blackbody measurements are made and the time test site measurements are made, which will result in poor calibration (see section IV). At the drop-off point the dewar is filled with liquid nitrogen. One filling of liquid nitrogen lasts approximately 4 hours. More recent versions of the instrument have an 8-hour dewar. Figure 1 illustrates the instrument assembled at a test site ready for measurement. The Gel Cell which powers the instrument provides sufficient charge to make approximately 5 measurements at each of -20-30 sites. Tile computer is powered by Nickel Cadmium batteries which typically last for about 5 measurements at each of approximately ten

sites. The number of site measurements that can be made with one set of batteries is significantly smaller if every spectrum is reduced to emissivity in the field.

Prior to making a measurement, the brightness temperature of the surface is obtained using an Everest Radiometer. This temperature is used to determine a suitable pair of blackbody temperatures for radiometric calibration (see Section IV). The cold blackbody and hot blackbody radiances are then measured. Spectra can be co-added in order to maximize signal-to-noise; co-adding 8 spectra produces a spectrum with no obvious noise while minimizing acquisition time. Each spectrum takes about 2-3 seconds to acquire; however, measurement of the blackbodies takes longer since the blackbody must be alternately heated and cooled to reach the specified temperatures. After measuring the blackbodies, the radiance from the sky is measured by placing a gold standard in the field of view. The standard has a reflectivity close to one so the majority of the radiation reaching the instrument has been reflected from the sky. If the emissivity of the gold standard is known, the sky radiation can be adjusted accordingly. However, if such an adjustment is included, the reflectivity of the field gold standard should be measured frequently against a laboratory gold standard for which contamination is minimized to identify any changes in the gold's reflectivity. This measurement can be undertaken using a laboratory interferometer or the μFTIR. This correction was applied to the data presented herein. The viewing tube of the fore-optics can be rotated so it is possible to measure the sky directly. However, such a measurement will be limited to ~50 around the zenith whereas the radiation from the gold standard has been integrated for all angles (see Section VI).

The radiance from the blackbodies and sky are measured first, and then the radiance from the target is measured. The number of measurements at a target varies depending on its apparent homogeneity, although 5 measurements are typically made. If the instrument temperature drifts by more than 0.2°C during the series clflllle:lslllrellle] -its, the blackbody measurements and sky measurements are repeated. Thea mount of drift in the instrument determines the accuracy of the recovered radiance (see section IV) , The sky measurement is also repeated if the sky "changes,'' although measurements are typically made only under near dear-sky conditions. It typically takes -20 minutes to calibrate the instrument, measure the sky radiation and make 5 measurements at a site.

IV. Radiometric Calibration

Radiometric calibration is the conversion of the instrument DN to radiance. It is achieved by measuring the blackbody at two known temperatures, one above and the other below the sample temperature. If the output numbers (D_λ) are linearly related to the input radiance (R_λ) then for a given wavelength:

$$R_\lambda = a + bD_\lambda \tag{1}$$

where a and b are constants that relate radiance to data number. If the radiance for the cold

blackbody (R_c) is given by:

$$R_c = P(\lambda, T_c) \tag{2}$$

and the radiance from the hot blackbody (R_h) by:

$$R_h = P(\lambda, T_h) \tag{3}$$

where $P(\lambda,T)$ is the Planck blackbody radiance. Then given R_c and R_h one can solve for a and b using Equation (1) with the following result:

$$a = \frac{R_h D_c - R_c D_h}{D_c - D_h}$$
$$b = \frac{R_c - R_h}{D_c - D_h} \tag{4}$$

Clearly equation (1) is sensitive to any non-linearity between (he input radiance and output data numbers. TCJ minimize any non-linearity the blackbody can be set at a temperature slightly below and slightly above that of the surface. The blackbody pair is typically chosen to be -5° C above and -50 C below the surface temperature reported by the Everest radiometers. This results in a good radiometric calibration of the sample but not of the sky which is much cooler than the sample (Note under clear sky conditions with low humidity the sky temperature is typically below -40° C). The +/- 50 range may need to be increased for materials with a strong emissivity contrast such as quartz, where the emissivity of the material may be sufficient to reduce the radiance from

the surface below that of a blackbody 5 degrees cooler than the broadband surface temperature. Korb et al., (*submitted, 1996*) adopt an alternate approach of setting the blackbody to its maximum and minimum possible values. This approach has been used for the demonstration spectrum of quartz but not for the field spectra. The advantage of measuring the blackbody at its minimum and maximum temperature (these will vary depending on sun-loading) is the minimum value is closer to the sky temperature (obtained with the gold standard) thereby reducing any errors in extrapolation of the calibration values to the sky measurement. The disadvantage of this approach is it takes longer than making the measurements slightly above and slightly below the sample temperature. With either approach the instrument should be re- calibrated if its temperature drifts by a few tenths of a degree, ideally if the instrument temperature changes at all, The optimum aproach in situations where the sky is not rapidly changing would be to first calibrate the sky measurement using the maximum and minimum settings of the blackbody then calibrating the sample using a set blackbodies that closely bracket its temperature. The sample blackbodies could be repeated if the instrument drifted but there would be no need to repeat the sky blackbodies provided the sky had not changed.

Figure 2 shows the raw output numbers for the cold and hot blackbodies and a sample of quartz. Note the double peak in the raw spectra that results from "doping" the I IgCdTe detector to increase its sensitivity at longer wavelengths. Figure 3 shows the calibrated quartz spectrum. The main quartz doublet around 8.5 μ m is clearly apparent as is the weaker doublet around 12.5 pm. The main doublet is strongly affected by atmosphere absorption and is very "noisy" in appearance. The removal of atmospheric effects is described in Section VI.

A variety of methods were developed to test the radiometric calibration) of the p FTIR. The methods utilize the external blackbody supplied with the μ FTIR, henceforth referred to as the p FTIR blackbody, and another external blackbody purchased from Electro-Optics instruments (1301). The EOI blackbody has an absolute accuracy of 0.05 'C and can be set to any temperature +/- 0.01 °C. Other specifications for the EOI blackbody are given in Table 1.

The first method used to check the radiometric calibration consisted 01 measuring the energy from the μ FTIR blackbody at two temperatures, then twice measuring the energy from the EO1 blackbody at each of three temperatures (the two μ FTIR blackbody temperatures and an intermediate temperature). This was repeated for several pairs of μ FTIR blackbody temperatures between 30 and 60 °C. The μ FTIR blackbody measurements and EOI blackbody measurements for a particular blackbody pair were made within a time period of about 30 minutes. During each 30-minute measurement period the temperature inside the optical heart did not change, according to readout from the thermistor in the optical head. These results are summarized in Table 2. They indicate the smallest error in the recovered temperature is generally associated with the intermediate temperature with larger errors for the sample measurements that are close to the temperature of the blackbodies. The error in the recovered temperature of the intermediate measurement ranged between 0.34 and 0.59 °C. This indicates that the blackbody temperatures should be chosen such that the blackbody radiances bracket the radiance range of the surface.

The second method used to check the radiometric calibration of the μ FTIR consisted of measuring a single p FTIR blackbody pair for calibration, and then measuring the EOI blackbody

for a range of temperatures between 20 and 50° C over an extended period of time. During the period of measurement the reported instrument temperature increased from 23.30 C to 23.40 C, then decreased back 23.3 °C. The error in the recovered EOI blackbody temperatures and instrument temperature were plotted as a function of time (Figure 4). Examination of the figure suggests that a change in instrument temperature of one tenth of a degree is not strongly correlated with the error in the recovered temperature and that the error in the recovered temperature is about 0.5 'C even after 60 minutes of intermittant operation.

V. Spectral Calibration

The spectrum is sampled every 3.13 wavenumbers (wn) using a laser diode (780 nanometers). This results in a spacing between points of 0.011 pm at 6 μm and 0.080 μm at 16 μm. Unlike the classic moving mirror Michelson Interferometer, the μFTIR uses a set of crystals that slide past each other to create the interferogram. This provides a more compact design but the wavelength file must be corrected for dispersion of the crystals. The (dispersion correction is based on a formula derived through a laboratory calibration at Designs and Prototypes. The laboratory calibration involves measuring the spectrum of polystyrene which contains spectral features at known wavelengths. Features at 3, 8 and 11 pm are used for the spectral calibration. In order to check the accuracy of the dispersion correction a spectrum was acquired from the gold standard under clear sky conditions. A model sky spectrum, at various resolutions, was then calculated and the wavelength positions of distinct water-vapor lines in the model spectra compared with those in the measured spectrum (Figure 5). The model and measured wavelengths of several of the features are given in Table 3. These data indicate the error is less than 1 wavenumber. Since a sky

spectrum is measured at every locality this method of using known water vapor lines for spectral calibration provides a means for continually monitories the spectral calibration of the instrument. It should be noted that the water-vapor features are only well developed in the 8-9 μm region and therefore our proof of the spectral calibration is only valid in this region since the spectral calibration is non-linear with wavelength. Furthermore, the misalignment of the second quartz doublet between the spectrum measured with the Nicolet laboratory interferometer and the μFTIR (Figure 7) suggests there are spectral calibration problems in the μFTIR data at the longer wavelengths. The spectral calibration does not vary over time so when a new correction procedure is developed it can be applied to any existing data acquired with the instrument.

VI. Atmospheric Correction

The radiance at the instrument (L_λ) is given by:

$$L_\lambda = [\epsilon_\lambda L_{bb\lambda}(T) + (1 - \epsilon_\lambda) L_{sky\lambda}] \tau_{A\lambda} + L_{V\lambda} \quad (5)$$

where:

ϵ_λ = Surface emissivity at wavelength λ.

$L_{bb\lambda}(T)$ = Spectral radiance from a blackbody at surface temperature (T).

$L_{sky\lambda}$ = Spectral radiance incident upon the surface from the atmosphere.

$\tau_{A\lambda}$ = Spectral atmospheric transmission,

$L_{V\lambda}$ = Spectral radiance from atmospheric emission and scattering that reaches the sensor.

Since we are close to the surface the spectral transmission] and spectral radiance from the atmospheric emission and scattering terms can be ignored. If we then assume the gold standard has an emissivity equal to zero, the radiance measured from the gold standard is equal to the spectra] radiance incident upon the surface from the atmosphere ($L_{sky\lambda}$). In reality the emissivity of the gold standard may be slightly greater than zero and the radiance from the standard can be adjusted accordingly. The spectra presented herein were corrected for the non-zero emissivity of the gold standard. The emissivity is derived by subtracting $L_{sky\lambda}$ (obtained by measuring the gold standard) from tile measured surface radiance (equation S):

$$\epsilon_\lambda = \frac{L_\lambda - L_{sky\lambda}}{L_{bb\lambda}(T) - L_{sky\lambda}} \qquad (6)$$

In order to apply equation (6) it is necessary to know the temperature of the surface. This is obtained by assuming the emissivity is constant in a given wavelength range and inverting the Planck equation for each wavelength in that range. Ideally the temperatures derived for all the wavelengths where the emissivity is assumed equal to 1 .() should be identical. In reality, there may be some difference due to noise in the system or emissivity variations within the wavelength range. Also if the surface is textured there may be some surface temperature variations as a result of shadowing. Generally the emissivity is assumed constant in the 7.7-7.8 pm region where silicate minerals typically have their Christianson frequency, and where the emissivity is very close to 1.0. For non-silicate materials this assumption may bc erroneous. For example, this assumption for a carbonate would be incorrect, the emissivity of a carbonate is fairly constant but not equal to

1.0 in this region. In the software provided with the instrument, the maximum temperature within the range is selected. In the complementary software developed at the Jet Propulsion Laboratory a series of blackbodies are fitted to the data points between the maximum and minimum temperatures for the region and the blackbody with the best least-squares tit utilized. All spectra presented in this paper utilize the software developed at the Jet Propulsion Laboratory. The maximum-temperature approach is very sensitive to any noise, whereas the least-squares fit approach is less sensitive to noise but sensitive to any variation in emissivity in the range where the emissivity is assured constant. If the emissivity is constant, known and not equal to 1.0 the known constant should be used instead. In the case of the carbonate example mentioned above if the emissivity is assumed equal to 1.0 the emissivities reported for the entire spectrum will be too high. The apparent emissivity (which is simply the ratio of the measured reliance to a blackbody at the same temperature as the surface) using the method outlined above to determine the temperature for the same sample of quartz, is shown in Figure 6. The spectrum appears noisy, particularly the main quartz doublet, clue to atmospheric effects. The true emissivity utilizing the method outlined above to remove the reflected atmospheric downwelling radiance is shown in Figure 7 (Field, corrected gold). The atmospheric lines within the doublet are now suppressed and in addition the main doublet is deeper due to the removal of the "filling in" effect of the reflected sky radiance which adds radiance from the sky in areas where the emissivity is less than 1.0 (Equation 5). The amount of radiance added increases as the emissivity decreases. Fortunately the feature is not completely "filled in" since the sky is much colder than the surface and therefore less radiance is added. However, if the sky were at the same temperature as the surface the feature would be completely filled in and the spectrum would be that of a blackbody. This explains why

samples should be heated when the instrument is used in the laboratory where the surface, ambient air, and radiating surfaces (walls) are all at approximately the same temperature. Figure 7 also shows the spectrum that is derived for the quartz sample with the μFTIR if there is no compensation for the non-zero emissivity of the gold standard (Figure 7 - Field, uncorrected gold). The depth of the main quartz doublet in the Field spectrum with correction for the non zero emissivity of the gold is greater indicating that if this is not taken into account the sky correction will overcompensate for the reflected sky radiation.

Figure 7 also shows spectrum of the same quartz sample measured using our laboratory interferometer with a hemispherical reflectance attachment. The laboratory reflectance spectrum was converted to emissivity using Kirchhoff's Law ($1-\epsilon = R$). It is tempting to use these spectra to validate Kirchhoff's Law (Salisbury et al., 1994), However, caution should be applied since any errors in the surface temperature derived for the field spectrum, utilizing the method outlined above, will cause the absolute value of the true emissivity spectrum to increase or decrease and also cause the spectrum to tilt depending on whether the surface temperature has been under-or over-estimated. This comparison also indicates that the spectra] calibration of the field instrument is poor at longer wavelengths around the position of the second quartz doublet.

VII. Example Spectra

The spectrum of pure quartz used to illustrate the reduction of data acquired from μFTIR provides an indication of the potential of the instrument, However, in reality most surface exposures of minerals are not pure and any spectral features may be suppressed or complicated by

factors such as soil development and vegetation. Figures 8, 9 and 10 provide some spectra from field measurements of natural surfaces in Death Valley, California, Mt Fitton, South Australia and Iron Hill, Colorado respectively in 1994. Figure 11 illustrates vegetation spectra from all three localities. All spectra were acquired under clear skies with surface temperatures ranging from -10° Cto 50°C.

The spectra for thenardite (Na_2SO_4), halite (NaCl), gypsum ($CaSO_4$), and basalt are shown in Figure 8. Thenardite is characterized by a well developed doublet centered on 8.5 µm. 13y contrast gypsum has a single feature centered on about the same wavelength as thenardite. If areas of thenardite and gypsum are imaged by an instrument with a similar configuration to TIMS it is possible to discriminate the areas of gypsum from the areas of thenardite. However, the spectral resolution of TIMS is insufficient to permit the identification of either gypsum or thenardite. This is possible with the µFTIR spectra. The spectrum of halite is flat in the thermal infrared and its common occurrence in playas make it a good calibration target, although it can show spectral features if it contains any fluid inclusions or other minerals suspended within it. The spectrum of basalt, a dark-colored extrusive igneous rock commonly composed of feldspar and pyroxene (Bates and Jackson, 1984), is characterized by a broad minimum cent ered around 9.3 µm and referred to as the reststrahlen band. This band occurs at snort wavelengths (around 8.5 µm) for rocks dominated by framework silicates (e.g. quartz, feldspar) and progressively longer wavelengths for silicate rocks with more abundant sheet (e. g. mica), chain (e.g. pyroxene and amphibole) and isolated SiO_4 tetrahedra (Hunt, 1 980). These spectra were acquired as part of a st udy of the use of remotely sensed TIMS data for mapping variations in the evaporitic minerals in

the floor of Death Valley (Crowley and Hook, 994; Crowley and Hook, 1995).

The spectra of granite, dolomite ($Ca(Mg,Fe)(CO_3)_2$, tremolite ($Ca_2(Mg,Fe)_5(OH)_2(Si_4O_{11})_2$), talc ($Mg_3(OH)_2(Si_2O_5)_2$), epidote ($Ca_2(Al,Fe)_3(OH)(SiO_4)_3$ and a mafic dike are shown in Figure 9. Granite, a plutonic rock dominated by quartz and feldspar (Bates and Jackson, 1984), has a more complicated mixed miners] spectrum (Figure 9). The spectrum of dolomite has a distinctive emission minimum around 11.1 µm. This minimum shifts to slightly longer wavelengths if calcite rather than dolomite is present (Salisbury and D'Aria, 1992). The detection of this shift with TIMS remains ambiguous but any shift would clearly be apparent in µFTIR spectra provided the instrument had good spectral calibration. Tremolite is characterized by a fairly complex spectrum but it would still be possible to identify the presence of dolomite in samples of tremolite since these minerals have diagnostic emission features in different parts of the thermal-infrared spectrum . The spectrum of talc is characterized by an asymmetric doublet with the main feature centered around 9 pm. Talc is mined at Mount Fit ton and data from the µFTIR could be used to aid in the exploration for similar deposits elsewhere. Talc is graded according to its purity with the presence of silica reducing its value. Clearly, the µFTIR data could be used to evaluate the abundance of both talc and quartz (silica), Epidote displays a variety of feature in the thermal infrared whereas the mafic dike is characterized by a single feature around 9.4 µm. The mafic dike has a basaltic composition. These data were acquired as part of a joint study between the Commonwealth Scientific Research Organization (CSIRO) and Jet Propulsion Laboratory to evaluate the combined use of the CSIRO rapidly tuned profiling CO_2 laser with -100 channels between 9 and 11 µm with the TIMS (Cudahy *et al.* 1994).

The spectra of granite, uncompahgrite, biotite ($K_2(Mg,Fe)_2(OH)_2(AlSi_3)_{10}$), riebeckite ($Na_2Fe^{II}_3Fe^{III}_2(Si_8O_{22})(OH,F)_2$), and carbonatite are shown in Figure 10. The spectrum of granite is a mixed mineral spectrum and is included to demonstrate some of the diversity in the spectral signatures of granites (see also Figure 9). Uncompahgrite is a sodium-rich rock but this particular sample was dominated by calcite. The presence of calcite is indicated by a small feature around 11.2 µm. Note the slightly longer wavelength of this feature than in the dolomite (Figure 9). Biotite is characterized by a broad emission minimum centered around 9.9 µm. The spectrum of Riebeckite, a sodium amphibole is fairly complex with multiple minima. The spectrum of carbonatite is characterized by a single sharp feature at 11.1 µm indicating the carbonatite is dominated by dolomite rather than calcite. These spectra were acquired as part of a study to use TIMS data to map the geology and mineralization of the Iron Hill, area (Watson *et al.* 1995).

Figure 11 illustrates vegetation spectra from all three localities. At the spectral resolution and sensitivity of this instrument the spectra are fairly flat. It should be noted that reflectance measurements of vegetation indicate it is a graybody with an emissivity of 0.985 (Salisbury and D'Aria, 1992), however, with the data reduction method used here any graybody spectrum will have an emissivity of 1.0. In the case of the Mount Fitton and Death Valley vegetation spectra, noise in the spectrum in the blackbody fit region results in the spectra having an emissivity around 0.99. The emissivity of the Iron Hill vegetation spectrum is very near to 1.0 due to the spectrum being noise free and the fact that the data reduction method causes all spectra that are graybodies to have emissivities equal to 1.0.

VIII. Summary and Conclusions

in order to validate the conclusions drawn from airborne and spaceborne remotely sensed multispectral thermal-infrared data, it is necessary to make similar measurements on the surface. The p FTIR instrument has been developed by Designs and Prototypes based on specifications provided by the Jet Propulsion Laboratory and Dr. J. W. Salisbury, in order to make these measurements.

Although it is now operational, there are still several aspects of the instrument that need to be improved. These include internal radiometric calibration, improved spectral calibration and the use of a Sterling Cycle cooler instead of liquid nitrogen. The advantage of internal calibration is that cooling and heating of a partial-aperture internal blackbody would be much faster. This would reduce the time it takes to produce a set of calibrated measurements since currently it takes several minutes for the blackbody to heat or cool to the appropriate temperature for calibration. The spectra] calibration should be improved such that the error is better than ± 1 wn across the 7-14 μm region. The primary advantage of a Sterling Cycle cooler is that it would be battery powered, and it is often difficult to obtain liquid nitrogen in remote regions.

In summary the p FTIR provides the first lightweight, calibrated, robust, high-resolut ion field instrument for validating multispectral thermal-infrared data.

Acknowledgments

The research described in this paper was carried out in part at the Jet Propulsion Laboratory, California Institute of Technology, under a contract with tile National Aeronautics and Space Administration as part of the Earth Observing System Mission to Planet Earth Program.

Special thanks go to Jack Margolis and Mike Abrams at the Jet Propulsion laboratory, for reviewing this manuscript and providing many helpful suggestions during the course of this work. Thanks also go to Alan Gillespie, Andy Korb, Jack Salisbury, and other anonymous reviewers whose suggestions significantly improved this manuscript.

Reference herein to any specific commercial product, process, or service by trade names, trademark, manufacturer or otherwise does not imply endorsement by the United States or the Jet Propulsion Laboratory, California institute of Technology.

References

Bates, R. L. and J. L. Jackson eds. 1984. *Dictionary of Geological Terms.* Anchor Press/Doubleday, Garden City, New York.

Crowley, J. K. and I look, S. J. 1994. Evaluation of Thermal Infrared Mult ispectral Scanner (TIMS) Data for Mapping Playa Evaporite Minerals in Death Valley, California. *Tenth Thematic Conference on Geological Remote Sensing*, San Antonio, Texas, USA, 9-12 May.

Crowley, J. K. and Hook, S. J. 1995. Thermal Infrared Multispectral Scanner (TIMS) study of playa evaporite minerals in Death Valley, Califoi nia. Submittal *Journal of Geophysical Research.*

Cudahy, T. J., Connor, P. M., Haushnecht, P., Hook, S. J., Huntington, J. F. Kahle, A. B., Phillips R. N. and Whitbourn, L. B. 1994. Airborne Silicate Mineral Mapping in Australia Using CO2 Laser and TIMS data. *Tenth Thematic Conference on Geological Remote Sensing*, San Antonio, Texas, USA, 9-12 May.

Hoover G. And A. B. Kahle 1987. A Thermal Emission Spectrometer for Field Use. *Photogrammetric Engineering and Remote Sensing*. 53:627-632.

Hunt, G. R. (J 980), In *Remote Sensing in Geology,* (B. S. Siegal and A. R. Gillespie Eds.) John Wiley and Sons, New York, Chap. 1.

Korb, A. R, Dybwad, P, Wadsworth, W. and Salisbury, J. W. Portable FTIR Spectroradiometer for Field Measurements of Radiance and Emissivity. Submittal *Applied Optics.*

Salisbury, J. W., First use of a new portable thermal-infr ared spectrometer 1990. *Proceedings of the Tenth Annual IEEE International Geoscience and Remote Sensing Symposium*, The Institute of Electrical and Electronic Engineers, New York, pp. 1775-1778.

Salisbury, J. W. and D'Aria, D. M. 1992. Emissivity of Terrestrial Materials in the S- 14 pm Atmospheric Window. *Remote Sens. Environ.* 42:83-106.

Salisbury, J. W., Wald, A. and D'Aria, D. M. 1994. Thermal-Infrared Remote Sensing and Kirchhoff's Law: 1 I .aboratory Measurements. Submitted *Journal of Geophysical Research.*

Tulloch, M, H. 1994. Ground-Truth Spectrometry Verifies Overnight Mapping. *Photonics Spectra, 28:18.*

Watson, K., Rowan, L. C., Bowers, '1'. L., Anton- Pacheco, C., Gumiel, P., and Miller, S. H. 1995. Lithologic analysis from thermal infrared data of the alkalic rock complex at Iron Hill, Colorado, In press, *Geophysics.*

Differential temperature range	-40 °C (o +40 "c
Absolute temperature range	-15°C to +65°C
Set point resolution	0.01 'C
Temperature display resolution	0.01 'C
Stability	± 0.01°C
Differential temperature accuracy	±0.03 °C to ±10 °C ±0.3% elsewhere
Absolute temperature accuracy	± 0.05 °C
Emissivity	0.99 ± 0.01
Surface area	*3ocm* x 30cm
Maximum area of aperture	24cm x 24cm
Power requirements	100/1 1<· *5/200/230* VAC, *50-400* Hz

Table 1. Specifications for the EOI Blackbody Radiation Source Model B]812D-2 and EOI Temperature Controller Model B2450E.

Blackbody (BB) Pair (°C)	Actual temperature (°C)	Recovered Temperature (°C)	Error
Cold BB = *30.1* Hot BB = *40.0*	**30.0**	29.54	0.46
	35.0	34.66	0.34
	40.0	39.16	0.84
Cold BB = 39.9 Hot BB = 49.9	40.0	39.38	**0.62**
	45.0	44.41	0.59
	50.0	49.47	0.53
Cold BB = 49.7 Hot BB = *59.6*	50.0	48.92	1.08
	55,0	54.49	0.51
	60.0	59.23	*0,77*

Table 2. Recovered temperatures from the EOI blackbody using three }11'"1'11< blackbody pairs (30,40°C), (40,50°C) and (50,60°C).

Feature	Micrometers		Wavenumber		Error (wn)	Error (μm)
	Model	μFTIR	Model	μFTIR		
A	8.921	8.918	1120.95	1121.33	-0.38	0.003
B	8.799	8.796	1136.49	1136.88	-0.39	0.003
C	8.514	8.515	1174.54	1174.4	0.14	-0.001
D	8.425	8.426	1186.94	1186.8	0.14	-0.001
E	8.347	8.338	1198.04	1199.33	-1.29	0.009
F	8.251	8.252	1211.97	1211.83	0.15	-0.001
G	8.203	8.210	1219.07	1218.03	1.04	-0.007
H	8.163	8.168	1225.04	1224.29	0.75	-0.005

Table 3. Position of water vapor lines shown in Figure 5 (A-G) in wavenumber and micrometers for a model sky spectrum and a sky spectrum measured with the μFTIR. Also shown is the difference between the model and measured value for each water vapor feature in wavenumbers and micrometers.

List of Figures

Figure 1. Photograph of the Jet Propulsion Laboratory μFTIR in Death Valley, CA during the 1994 Field Campaign. The gray box on top of the tripod is the optical head and the briefcase which includes the computer the system unit.

Figure 2. Raw output numbers for the cold and hot blackbodies and a sample of quartz.

Figure 3. Calibrated quartz spectrum shown in Figure 2.

Figure 4. Error in recovered temperature and instrument temperature versus elapsed time..

Figure 5. Model spectra for a clear sky calculated at resolutions of 2 and 4 wavenumbers (upper curves) and a sky spectrum acquired by the μFTIR (lower curve). Letters A-F identify peaks whose wavelength and wavenumber are given in Table 2.

Figure 6. Apparent emissivity for a sample of quartz. The apparent emissivity is the ratio of the measured radiance to the radiance of a blackbody at the same temperature as the measured radiance. The blackbody temperature is obtained by assuming the emissivity is equal to 1,0 in some wavelength range in the measured temperature spectrum, then inverting Planck's equation at that wavelength to obtain the temperature. In this spectrum the emissivity was assumed equal to 1.0 in the wavelength range 7.7 to 7.8 μm.

Figure 7. Laboratory reflectance spectrum of the quartz sample measured with a Nicolet Spectrometer. The laboratory spectrum has been converted to emissivity using Kirchhoff's Law ($1 - \epsilon = R$). Emissivit y spectrum of the quartz. sample measured with the p FTIR, including compensation for non-unity reflectance of gold (corrected gold). The temperature of the sample was obtained using the method outlined with Figure 6 and calibrated data processed using equation (7). Note the absence of atmospheric lines within- and the increased depth of- the quartz doublet compared to Figure 6. Emissivity spectrum described above without the correct ion for the non- unit y in reflectance of the gold standard.

Figure 8. Example spectra of thenardite (l'), halite (H), gypsum (G) and basalt (B) measured in Death Valley, CA in 1994. Spectra are offset for clarity.

Figure 9. Example spectra of granite (G), dolomite (D), tremolitic dolomite (Tr), talc (Ta), epidote (E) and a mafic dike (MD) measured at Mount Fitton, Australia in 1994.

Figure 10. Example spectra of granite (G), uncompahgrite (U), biotite (B), riebeckite (R) and carbonatite (C) measured at iron Hill, CO in 1994.

Figure 11. Vegetation spectra from the previous three localities: Death Valley, CA (DV), Mt Fitton (MF) Australia and iron Hill, CO (IH) measured in 1994.

Fig 1 2-27-95

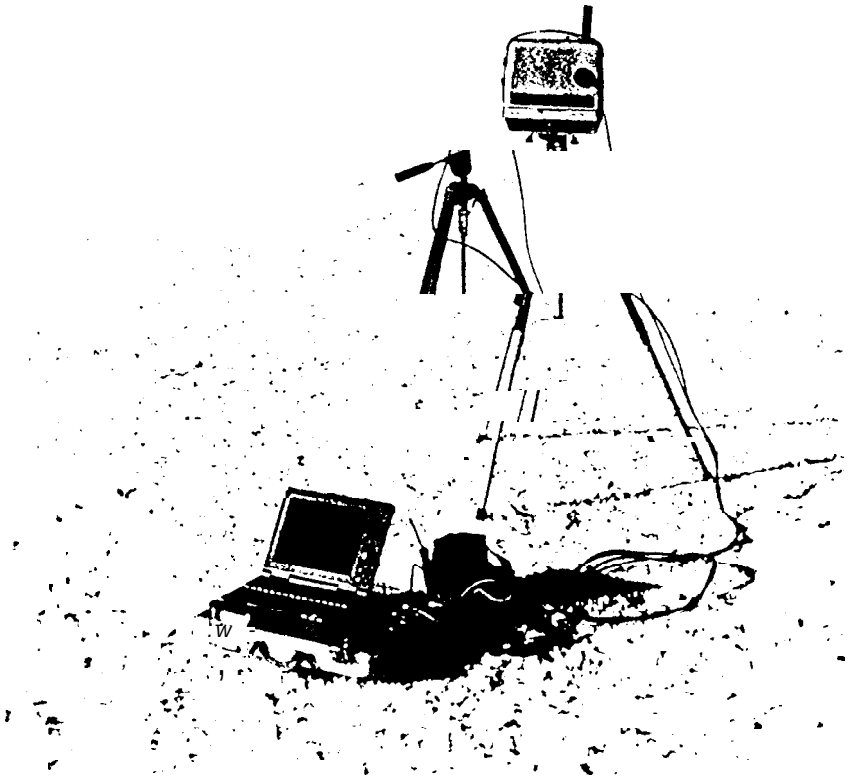

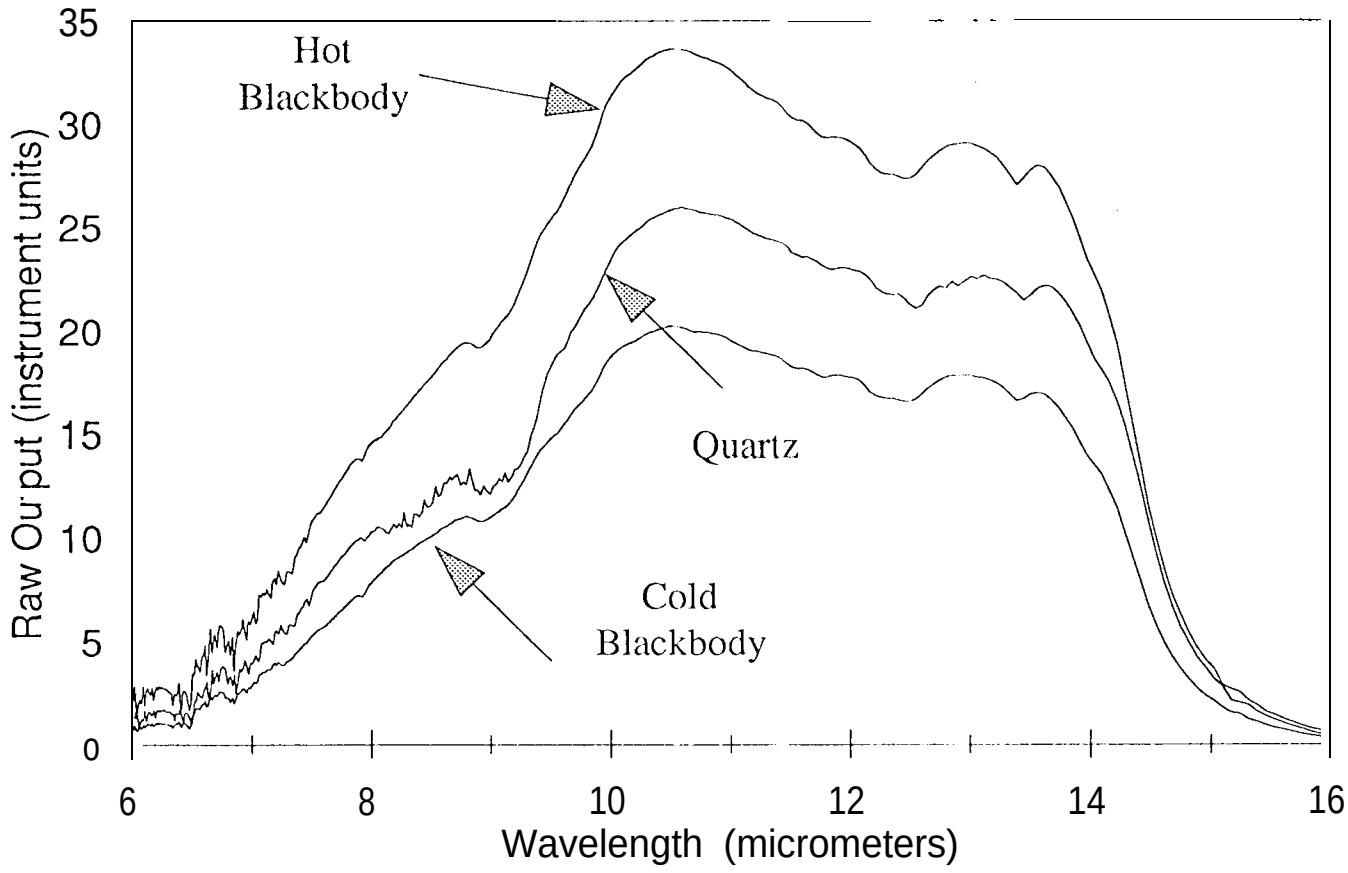
Hot
Blackbody
Quartz
Cold
Blackbody
Raw Output (instrument units)
35
30
25
20
15
10
5
0
6
8
10
12
14
16
Wavelength (micrometers)

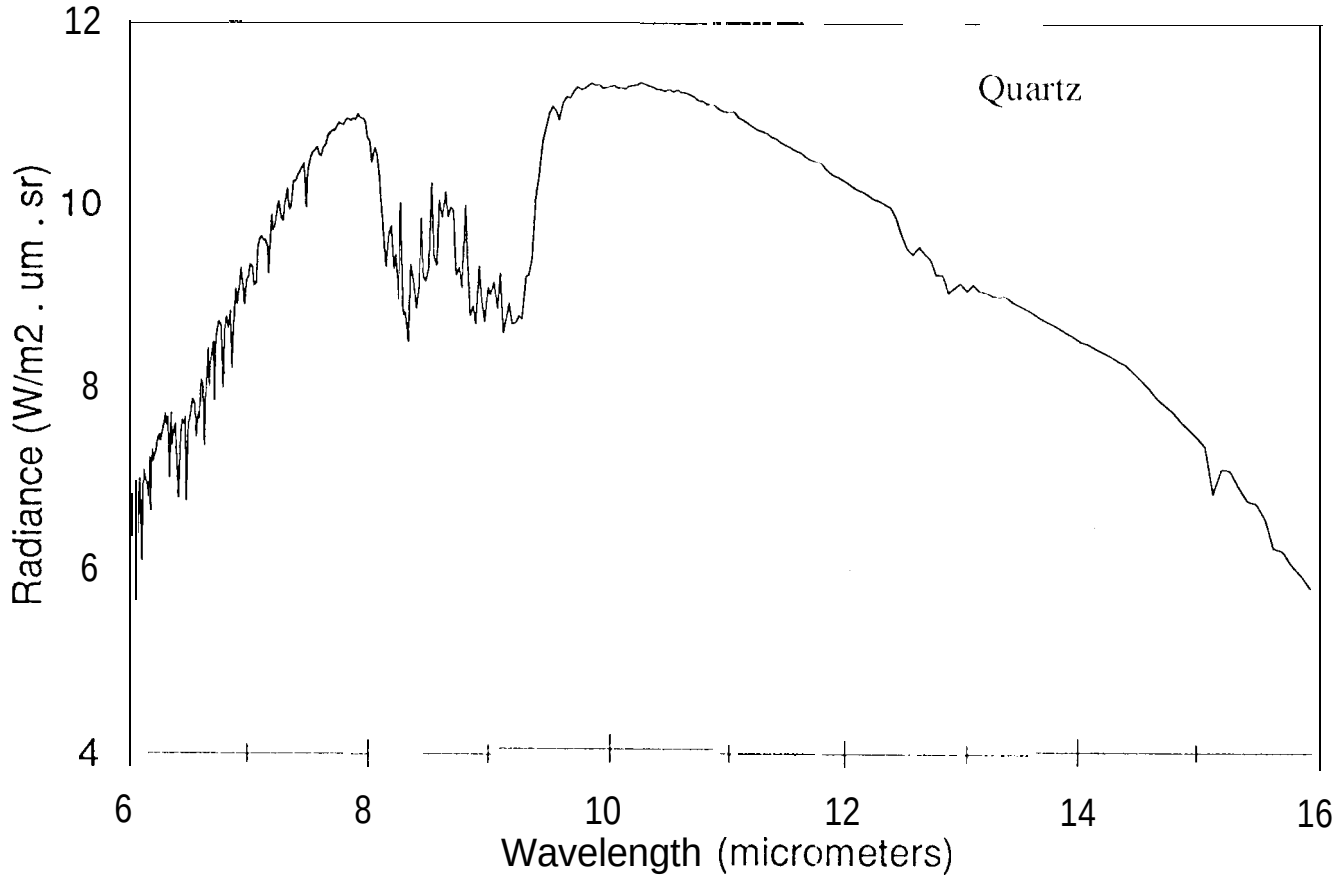
Quartz
Radiance (W/m2 . um . sr)
12
10
8
6
4
6
8
10
12
14
16
Wavelength (micrometers)

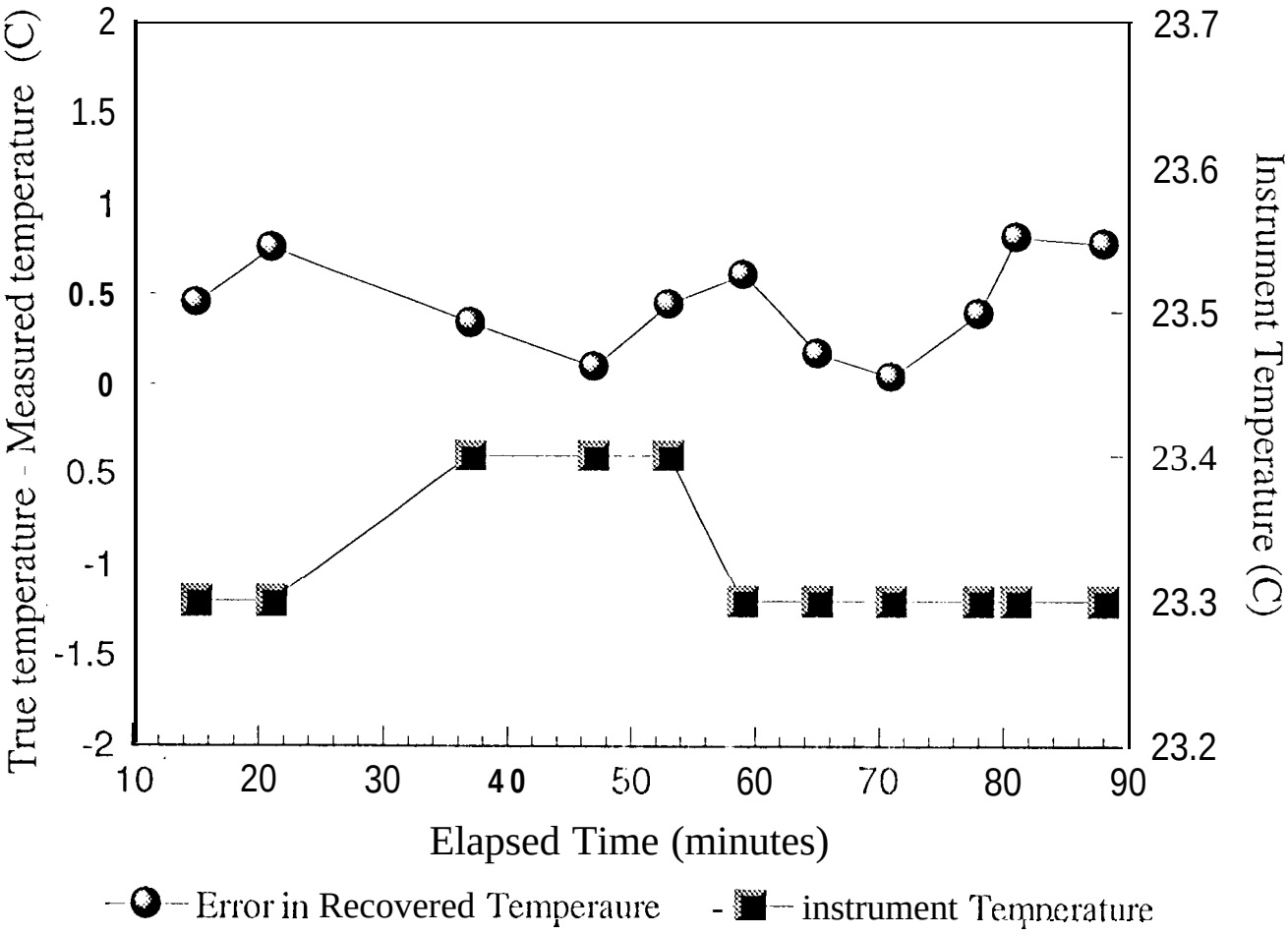
True temperature - Measured temperature (C)
2
1.5
1
0.5
0
0.5
-1
-1.5
-2
10
20
30
40
50
60
70
80
90
Elapsed Time (minutes)
23.7
23.6
23.5
23.4
23.3
23.2
Instrument Temperature (C)
Error in Recovered Temperaure
instrument Temperature

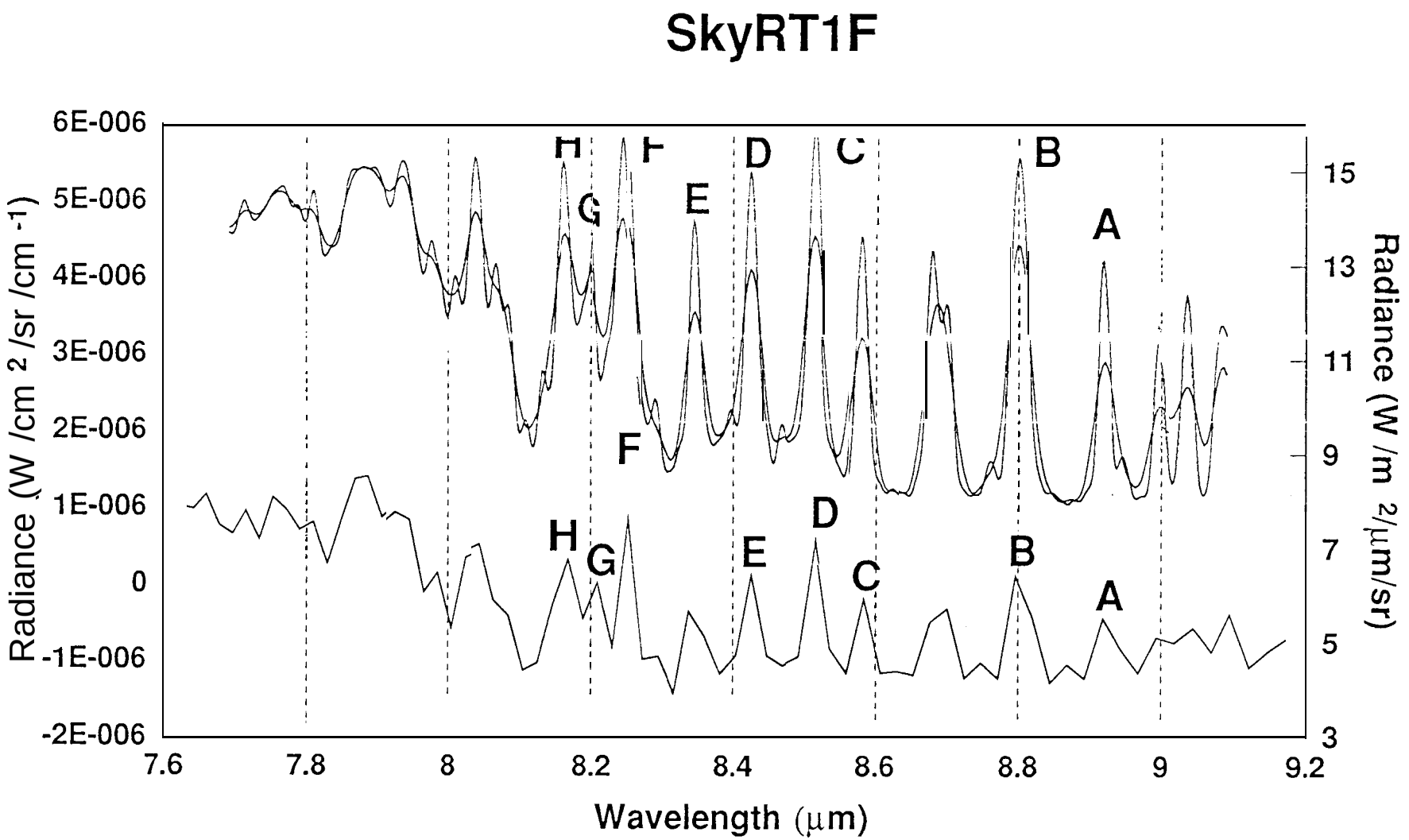
SkyRT1F
Radiance (W /cm 2 /sr /cm -1)
6E-006
5E-006
4E-006
3E-006
2E-006
1E-006
0
-1E-006
-2E-006
Radiance (W /m 2/μm/sr)
15
13
11
9
7
5
3
7.6
7.8
8
8.2
8.4
8.6
8.8
9
9.2
Wavelength (μm)
H
G
F
E
D
C
B
A

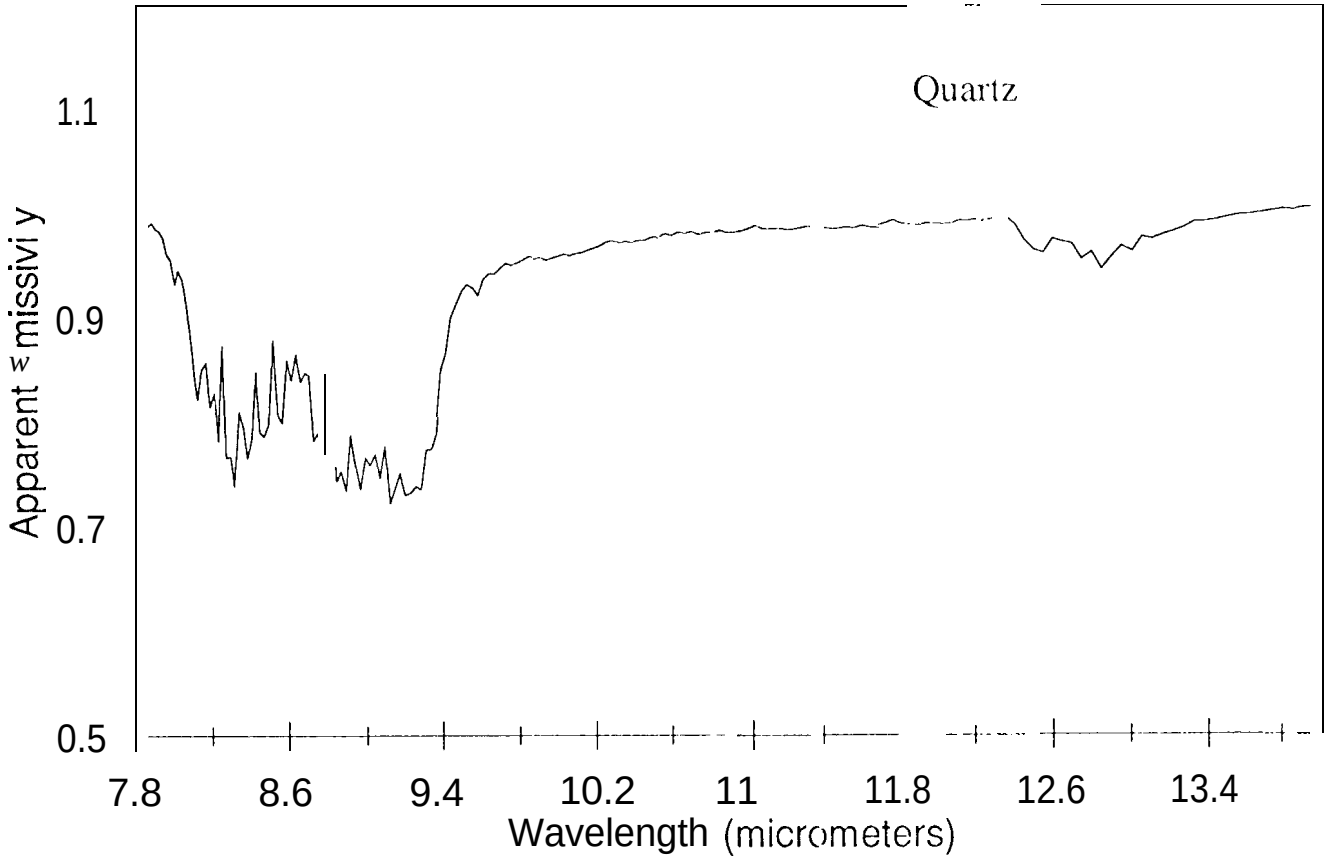
Quartz
1.1
0.9
0.7
0.5
Apparent ε missivi y
7.8
8.6
9.4
10.2
11
11.8
12.6
13.4
Wavelength (micrometers)

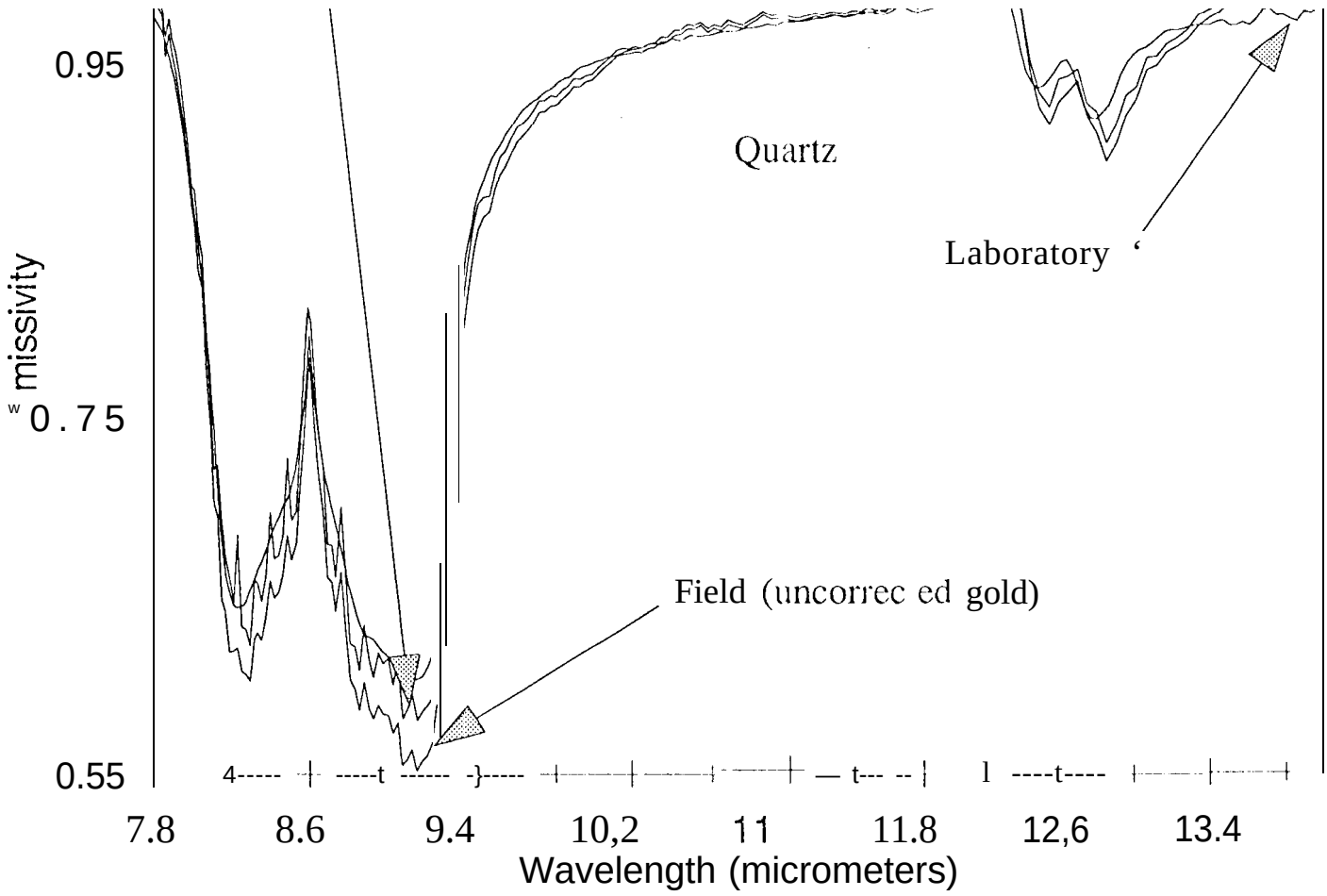
0.95
missivity
0.75
0.55
Quartz
Laboratory
Field (uncorrec ed gold)
7.8
8.6
9.4
10,2
11
11.8
12,6
13.4
Wavelength (micrometers)

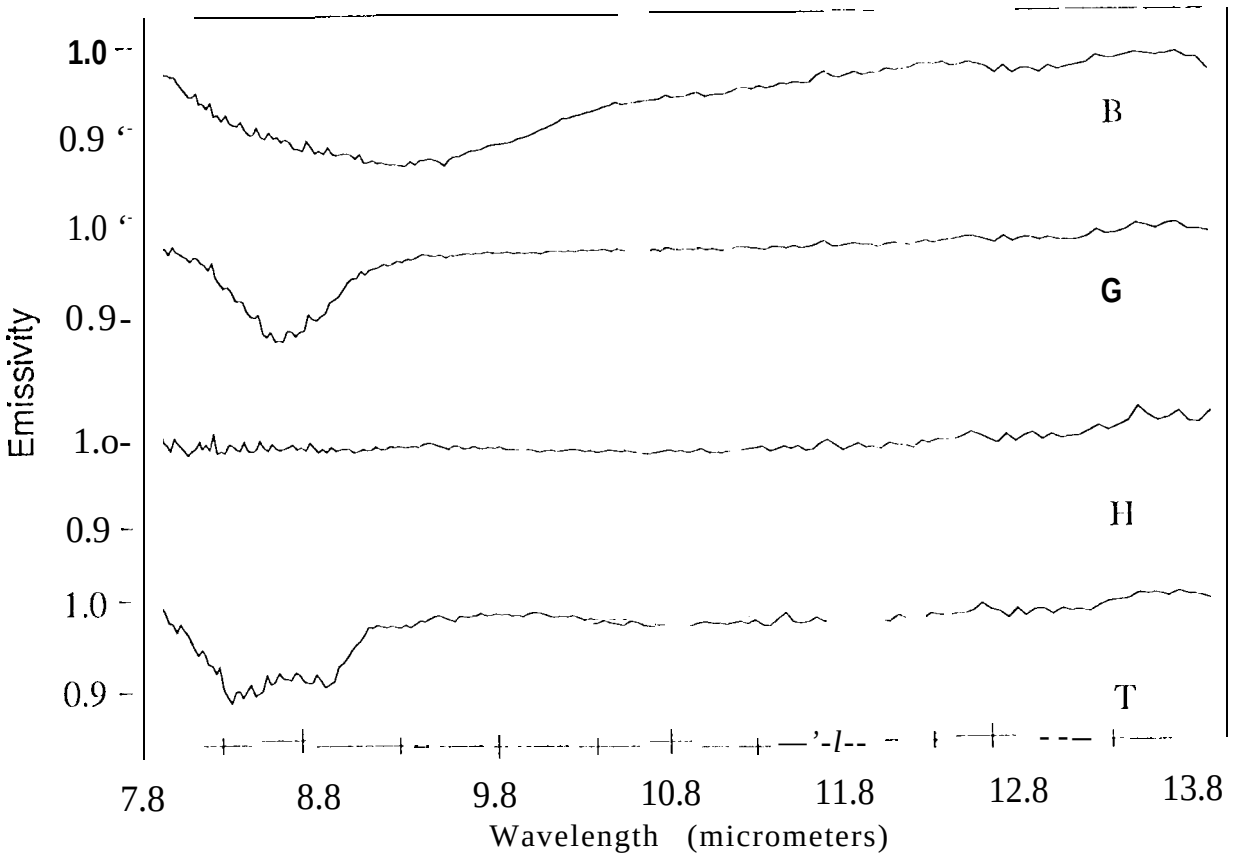
1.0
0.9
1.0
0.9
1.0
0.9
1.0
0.9
Emissivity
B
G
H
T
7.8
8.8
9.8
10.8
11.8
12.8
13.8
Wavelength (micrometers)

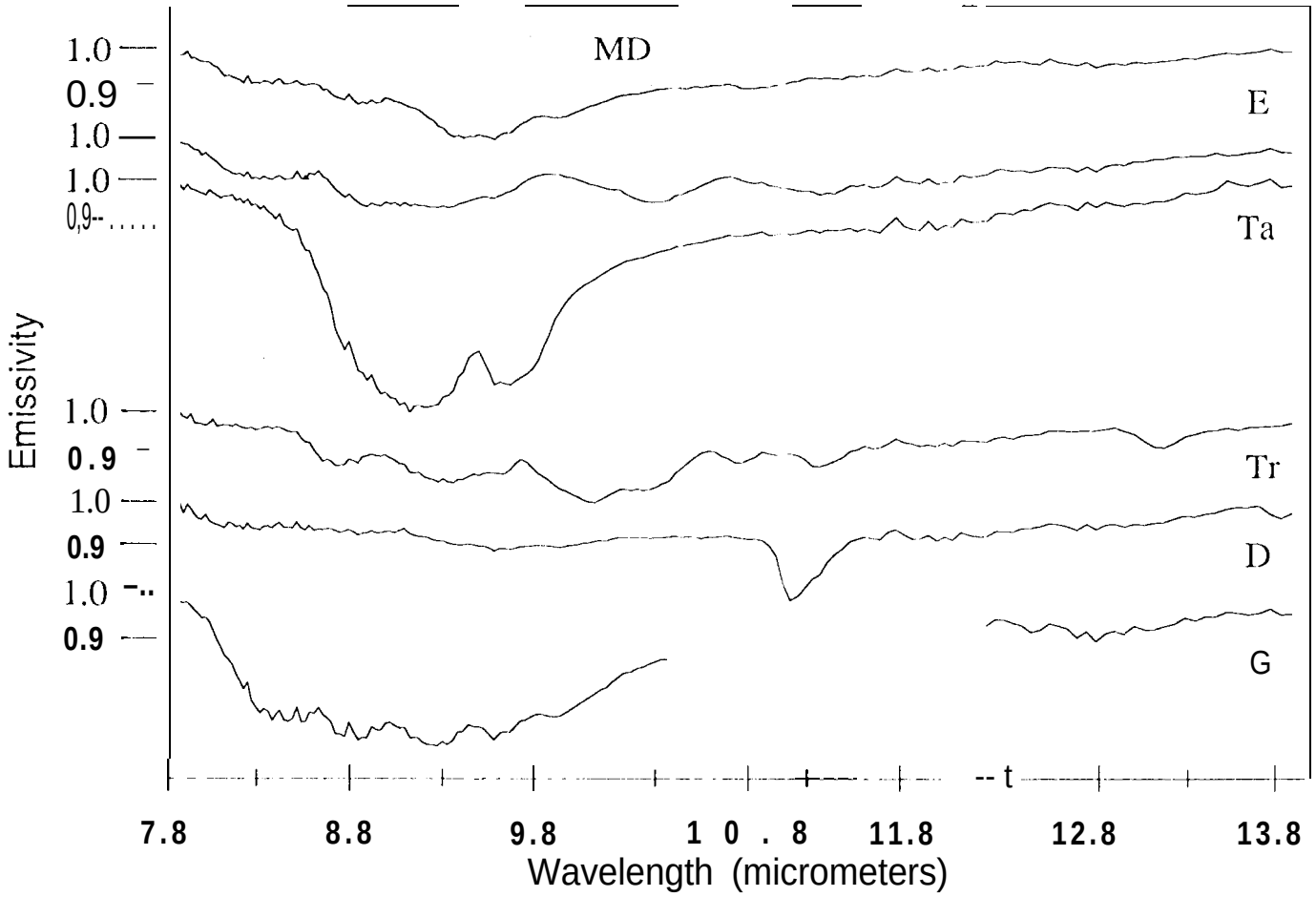
MD
E
Ta
Tr
D
G
Emissivity
1.0
0.9
1.0
1.0
0.9
1.0
0.9
1.0
0.9
1.0
0.9
-- t
7.8
8.8
9.8
10.8
11.8
12.8
13.8
Wavelength (micrometers)

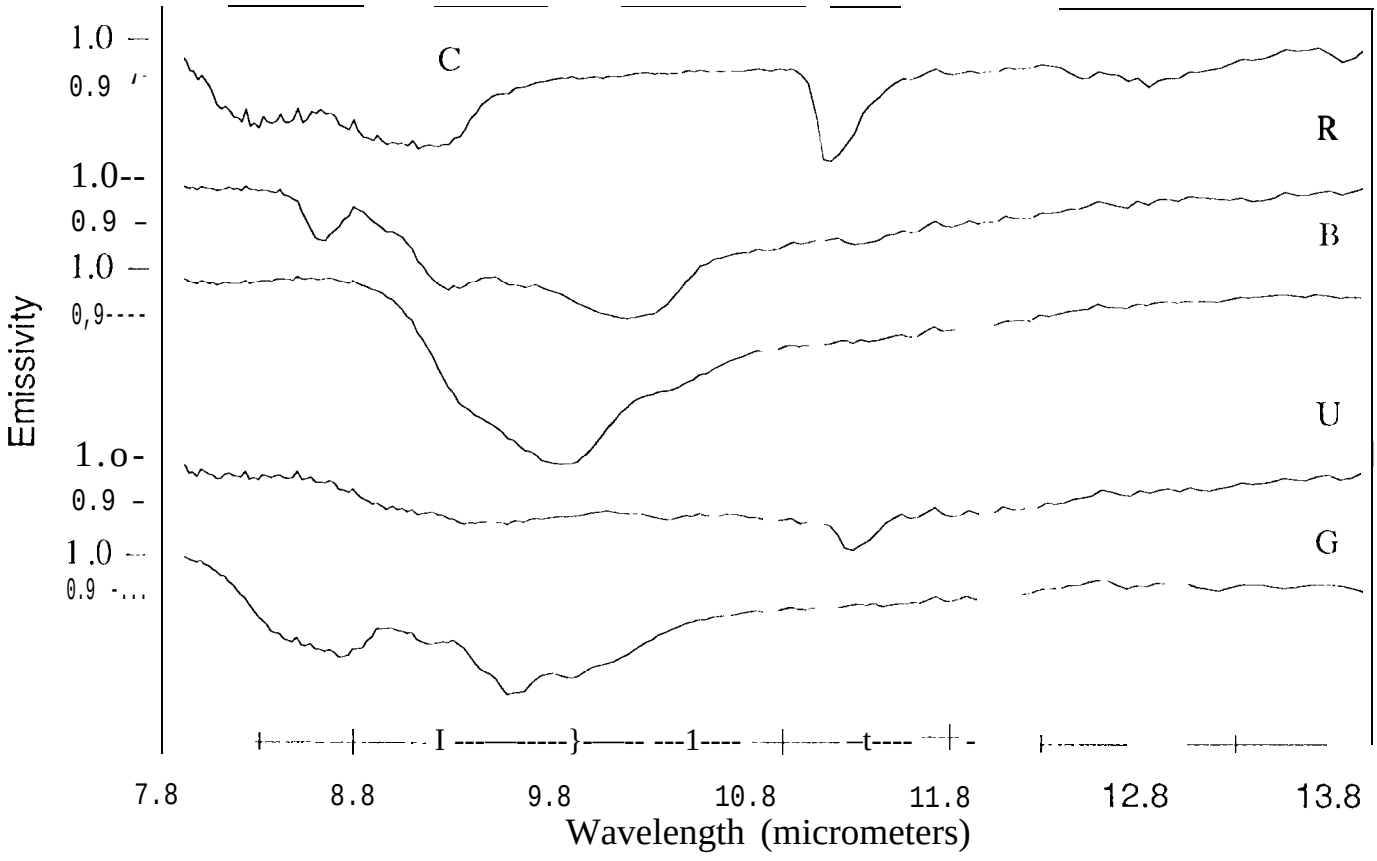
1.0
0.9
C
R
1.0
0.9
B
1.0
0,9
U
1.o
0.9
1.0
0.9
G
Emissivity
7.8
8.8
9.8
10.8
11.8
12.8
13.8
Wavelength (micrometers)